

Readout-power heating and hysteretic switching between thermal quasiparticle states in kinetic inductance detectors

P. J. de Visser,^{1,a)} S. Withington,² and D. J. Goldie²

¹*Kavli Institute of NanoScience, Faculty of Applied Sciences, Delft University of Technology, Lorentzweg 1, 2628 CJ Delft, The Netherlands and SRON National Institute for Space Research, Sorbonnelaan 2, 3584 CA Utrecht, The Netherlands*

²*Cavendish Laboratory, Cambridge University, JJ Thomson Avenue, Cambridge CB3 0HE, United Kingdom*

(Received 11 May 2010; accepted 20 October 2010; published online 7 December 2010)

A model is presented for readout-power heating in kinetic inductance detectors. It is shown that the power dissipated by the readout signal can cause the temperature of the quasiparticle system in the superconducting resonator to switch between well-defined states. At low readout powers, only a single solution to the heat balance equation exists, and the resonance curve merely distorts as the readout power is increased. At high readout powers, three states exist, two of which are stable, and the resonance curve shows hysteretic switching. The power threshold for switching depends on the geometry and material used but is typically around -70 dBm for Aluminum resonators. A comprehensive set of simulations is reported, and a detailed account of the switching process is given. Experimental results are also shown, which are in strong qualitative agreement with the simulations. The general features of the model are independent of the precise cooling function, and are even applicable for resonators on suspended, thermally isolated, dielectric membranes, where an increase in quasiparticle lifetime is expected. We discuss various extensions to the technique, including the possibility of recovering the cooling function from large-signal measurements of the resonance curve. © 2010 American Institute of Physics. [doi:10.1063/1.3517152]

I. INTRODUCTION

Kinetic inductance detectors (KIDs) are being developed extensively for large-format astronomical imaging.¹ They come in a variety of forms but the basic device comprises a microwave ($f_0 < 10$ GHz) superconducting thin-film resonator on a sapphire, quartz, or silicon substrate. The superconducting material is usually Al, Ta, or Nb, having a critical temperature, T_c , of approximately 1 K, 4 K, and 9 K, respectively. When an infrared, optical, or x-ray photon is absorbed, the surface impedance changes, and the resonant frequency shifts. By monitoring the transmission amplitude and phase, at a single readout frequency, highly sensitive detectors can be made. KIDs can be packed into large-format imaging arrays by lightly coupling thousands of resonators to a single, through transmission line, which can be read out using software-defined radio techniques.

A key issue when optimizing the performance of KIDs is decreasing the amount of noise. It is desirable to maximize the microwave readout power so that the transmission amplitude and phase can be recorded with a high signal-to-noise ratio, and the sensitivity of the detector is enhanced. In fact, when using phase readout, excess noise is seen, which scales inversely with the square root of power.^{2,3} This noise is often attributed to two-level systems, originating from the refractive index of the substrate or native oxide, fluctuating as a consequence of the movement of uncoordinated, lightly bound, atoms. Amplitude readout is sometimes used to minimize this problem.^{4,5} Unfortunately, as the readout power is increased above a certain threshold, the resonant curve be-

gins to distort, and eventually begins switching hysteretically as the readout frequency is swept up and down. This behavior is seen in all devices, although the exact power level at which the distortion appears varies from material to material. It can also vary between films of notionally identical material manufactured by different groups.

The power handling capability of superconducting resonators is also important from the point of view of detector linearity, because as the incident photon rate increases, the density of nonequilibrium quasiparticles increases.

In this paper, we present a model describing nonlinear behavior in KIDs due to microwave-readout heating. As power is applied, the temperature of the quasiparticle system rises until a balance is reached between the rate at which microwave energy is dissipated in the resonator, and the rate at which energy is transferred from the quasiparticle system of the superconductor to the phonon system of the substrate. We present simulations showing that our model accounts for the functional form of what is seen experimentally, and gives rise to multiple temperature states. These states manifest themselves as hysteretic switching in the resonance curves.

Nonlinearities in superconducting films and resonators are widely studied in the context of high- T_c superconductors for different applications,⁶ with critical temperatures ranging from 9 K (niobium) to 87 K (YBCO). Nonlinear behavior is found to originate from thermal instabilities due to local hot spots^{7,8} and vortices⁹⁻¹¹ leading to a power-dependent surface impedance.^{12,13} Other effects involve a Kerr nonlinearity¹⁴⁻¹⁶ or weak links in the film,^{17,18} leading to a nonlinear inductance at high current density. Intermodulation measurements can indicate which mechanism causes

^{a)}Electronic mail: p.j.devisser@tudelft.nl.

nonlinearities.^{14,19} In most mechanisms, the superconductor film quality plays a crucial role in the power handling.⁶

Quasiparticle heating is sometimes mentioned but neglected due to the relatively high thermal conductivity of high- T_c superconductors. Where thermal effects play a role, they are caused by local heating due to film inhomogeneities^{8,20} or measured by an external resonant probe.²¹ We emphasize that some of these effects may still be present in low- T_c resonators but the temperature-state switching described here is likely to dominate at the very low operating temperatures, $T_c/10$, of KIDs, especially where $T_c \approx 1-2$ K. Another global heating model, based on the substrate thermal conductivity, was previously described.²² Data presented in this reference was taken on resonators using more than 8 orders of magnitude more power and at temperatures from 40–70 K, which makes it a totally different regime than we study in this paper.

Nonlinear resonators can also be used for parametric amplifiers^{15,16} or intermodulation amplifiers.²³ This is usually done by introducing a nonlinear element in the resonator. The Josephson bifurcation amplifier is a well-known example. For a review, see Ref. 24, and references therein. Interestingly, this amplifier could be useful to enhance the sensitivity of the readout of KIDs.⁵

The paper is structured as follows: In Sec. II the proposed theory of readout-power heating in superconducting resonators is described, and then in Sec. III simulations are reported. In Sec. IV, experimental results are presented, which indicate that the simulations have the correct general forms. Finally, in Secs. V and VI we reflect on the findings and describe various ways in which the study might be taken forward.

II. THEORY

A. Superconducting microstrip resonators

The microscopic picture of the electrodynamic response of superconductors was developed by Mattis and Bardeen.²⁵ According to this theory, the complex conductivity, $\sigma = \sigma_1 - i\sigma_2$, describing the response of both Cooper pairs and quasiparticles to a time-varying electric field is given by

$$\frac{\sigma_1}{\sigma_N} = \frac{2}{\hbar\omega} \int_{\Delta}^{\infty} [f(E) - f(E + \hbar\omega)] g_1(E) dE + \frac{1}{\hbar\omega} \int_{\min(\Delta - \hbar\omega, -\Delta)}^{-\Delta} [1 - 2f(E + \hbar\omega)] g_1(E) dE, \quad (1)$$

$$\frac{\sigma_2}{\sigma_N} = \frac{1}{\hbar\omega} \int_{\max(\Delta - \hbar\omega, -\Delta)}^{\Delta} [1 - 2f(E + \hbar\omega)] g_2(E) dE, \quad (2)$$

where

$$g_1(E) = \frac{E^2 + \Delta^2 + \hbar\omega E}{(E^2 - \Delta^2)^{1/2} [(E + \hbar\omega)^2 - \Delta^2]^{1/2}}, \quad (3)$$

$$g_2(E) = \frac{E^2 + \Delta^2 + \hbar\omega E}{(\Delta^2 - E^2)^{1/2} [(E + \hbar\omega)^2 - \Delta^2]^{1/2}}, \quad (4)$$

and $f(E)$ is the Fermi function. σ_N the normal-state conductivity, and ω the angular frequency. To determine the conductivity as a function of temperature, it is necessary to know how the energy gap, $\Delta(T)$, changes with temperature. It can be calculated by numerically inverting the integral equation

$$\frac{1}{N(0)V_{sc}} = \int_{\Delta(T)}^{\hbar\omega_D} \frac{1 - 2f(\epsilon)}{\sqrt{\epsilon^2 + \Delta^2(T)}} d\epsilon, \quad (5)$$

where $N(0)$ is the single-spin density of states at the Fermi surface, V_{sc} is the scattering parameter or potential energy describing phonon exchange, \hbar is the reduced Planck's constant, ω_D is the Debye frequency, T is the temperature, ϵ the energy relative to the Fermi level, and k_B is Boltzmann's constant.

The surface impedance of a superconducting film can be calculated from the complex conductivity. For arbitrary thicknesses t , the surface impedance Z_s , in the dirty limit, is given by²⁶

$$Z_s = \sqrt{\frac{i\mu_0\omega}{\sigma}} \coth(\sqrt{i\omega\mu_0\sigma}t), \quad (6)$$

where μ_0 is the permeability of free space and σ the complex conductivity.

Knowing the geometry of the resonator, and the surface impedance as a function of temperature, it is possible to calculate the microwave loss as a function of temperature. Unfortunately, calculating the loss of a thin-film transmission line is more difficult than calculating the characteristic impedance and modal propagation constant, because it is necessary to know the detailed way in which the induced current penetrates into, and flows around, the waveguiding structure. To explore the basic properties of the model, it is beneficial to use a microstrip geometry so that we can take advantage of the equations developed by Yassin and Withington.²⁷ These equations, based on conformal mapping, allow the loss to be calculated accurately and analytically. Using them results in the propagation constant, $\gamma = \alpha + i\beta$, which includes the losses, and the characteristic impedance of the line, Z_0 .

The input impedance of a shorted transmission line, Z_{line} , is

$$Z_{line} = Z_0 \tanh \gamma l = Z_0 \tanh \left(\frac{\beta}{2Q_i} + i\beta \right) l, \quad (7)$$

where l is the length of the line. For an ideal line $\alpha=0$, and so when $l=\lambda/4$, the input impedance $Z_{line} \rightarrow \infty$. We have expressed the result in terms of the internal quality factor $Q_i = \beta/(2\alpha)$, which describes the losses. Obviously, an ideal line has an infinite Q_i .

The resonator is capacitively coupled at its open end to a readout line. A schematic of the relevant circuit components is given in Fig. 1. The capacitance of the gap, C_g , loads the resonator, and so at resonance the line is not exactly $\lambda/4$ long. Rather, resonance occurs when the capacitive impedance looking into the gap is equal in magnitude to the induc-

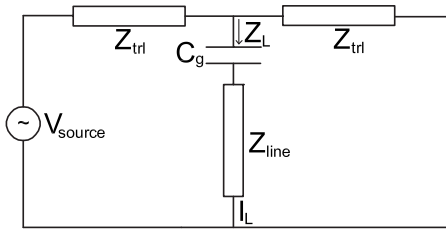


FIG. 1. Circuit schematic of the resonator, with Z_L the loaded impedance of the resonator, Z_{line} the resonator impedance without coupling gap, C_g the capacitance of the coupling gap, V_{source} the voltage of the source, I_L the current in the load, and Z_{trl} the impedance of the throughline.

tive impedance looking into the resonator. The total series impedance, as seen by the readout line, is given by

$$Z_L = \frac{1}{i\omega C_g} + Z_0 \tanh \gamma l, \quad (8)$$

where the second term is given by Eq. (7). In reality, the whole element consists of a through transmission line with the gap and resonator connected in parallel at some intermediate position. The forward scattering parameter between the input and output ports, S_{21} , becomes

$$S_{21} = \frac{2}{2 + Z_{trl}/Z_L}, \quad (9)$$

where Z_{trl} is the characteristic impedance of the through line and Z_L the impedance looking into the coupling gap, as given by Eq. (8). S_{21} can be written in terms of its amplitude $|S_{21}|$ and phase θ , according to $|S_{21}|e^{i\theta}$, which are the quantities recorded by the readout electronics.

B. Power dissipation

Now we are able to calculate the amplitude and phase of the resonance curve as a function of temperature. For temperatures well below T_c , the losses are exceedingly small but nevertheless finite, and therefore the resonator absorbs power. The quality factor of the resonator can be defined as $1/Q = 1/Q_c + 1/Q_i$, where Q_c is the coupling quality factor. At low temperatures, the Mattis and Bardeen theory predicts that the internal quality factor, Q_i , should increase exponentially as the temperature is lowered. Measurements show, however, the internal quality factor saturates at values of around 10^5 – 10^6 at $T/T_c \approx 0.2$ for our resonators, which means that an additional dissipative mechanism is present. The source of this loss may be due to excess quasiparticles,²⁸ loss at the surface of the superconductor, or in the dielectric material but the exact origin is not known.^{29,30} To make an improved estimate of the dissipated power, we take this saturation into account by modifying the internal quality factor in Eq. (7) by

$$\frac{1}{Q_i} = \frac{1}{Q_{i,MB}} + \frac{1}{Q_{sat}}, \quad (10)$$

where Q_{sat} is the saturation quality factor and $Q_{i,MB}$ the quality factor following the Mattis–Bardeen equations. In the calculations presented here we assume that the additional loss is due to quasiparticles, which is reasonable since we are inter-

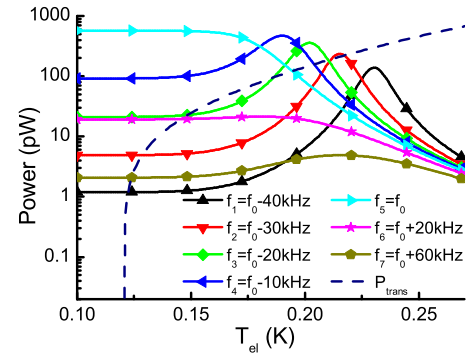


FIG. 2. (Color online) Power dissipated in an Al microstrip resonator as a function of temperature for different readout frequencies. The low temperature resonance frequency $f_0 = 4.263\,02$ GHz. The readout power is -57 dBm. The dashed line shows the electron-phonon cooling power as a function of temperature according to $P_{e-ph} = V \Sigma (T_{el}^5 - T_{ph}^5)$, for a phonon temperature of 120 mK.

ested in high readout powers, and dielectric loss saturates at power levels well before nonlinearities occur.^{30,31} This refinement is not central to the model, and changes the results very little but it does ensure that the model is consistent with what is seen experimentally.

Finally, we need to calculate the power dissipated in the resonator, which proceeds as follows. The power available from a microwave source, which we shall call the *readout power*, is taken conventionally to be

$$P_{readout} = \frac{V_{source}^2}{4Z_{trl}}, \quad (11)$$

where V_{source} is the Thévenin equivalent circuit voltage of the source. If this source is connected to the through transmission line of a KID, and the through line is terminated with a matched load, the current, I_L , flowing into the parallel component representing the coupling gap and resonator is given by

$$I_L = V_{source} \frac{Z_L}{Z_{trl}/Z_L + 2}, \quad (12)$$

where Z_L is the parallel load impedance, which is given by Eq. (8). Finally, the power dissipated in the load, P_{diss} , which is actually the power dissipated in the resonator because the coupling gap is lossless, is given by

$$P_{diss} = |I_L|^2 R_L, \quad (13)$$

where R_L is the resistance of the load, which is given by the real part of Eq. (8).

The dissipated power depends on how much power is coupled into the resonator, and therefore peaks at the resonant frequency. The resonant frequency is temperature dependent, and therefore the dissipated power is temperature dependent. In fact, we can define a resonant temperature for a particular readout frequency. This effect is shown in Fig. 2, where the dissipated power has been calculated for an Al microstrip resonator as a function of temperature, for different readout frequencies. The geometrical factors used in the simulation are listed in Table I, and the parameters of Al were taken to be $N_0 V_{sc} = 0.17$, $T_D = 420$ K, and

TABLE I. Parameters of the microstrip resonators simulated.

Parameter	Symbol	Value
Strip length	l	4 mm
Strip width	w	3 μm
Film thickness	t	200 nm
Dielectric height	h	200 nm
Gap capacitance	C_g	5 fF
Relative permittivity of dielectric	ϵ_r	11
Throughline impedance	Z_{trl}	20 Ω
Designed resonant frequency	f_0	4.263 02 GHz

$\rho=2.4 \mu\Omega \text{ cm}$.³² The simulations were carried out with a readout power of 2 nW (-57 dBm) and a bath temperature 120 mK.

We observe that the resonant temperature falls as the readout frequency is increased, as expected, because the resonant frequency always falls as the temperature is increased. At the highest readout frequencies, where the zero-temperature resonant frequency is approached, a plateau appears as a direct consequence of the saturation of the quality factor, Eq. (10).

C. Heat transport

The energy absorbed by the resonator leads to a heating of the quasiparticle system, which cools by transferring energy to the phonon system of the superconductor, and from the phonon system of the superconductor to the phonon system of the substrate. Equilibrium is established, for a particular readout frequency and readout power, when these rates are equal. The rate of heat loss will certainly increase as the temperature of the quasiparticles increases relative to that of the phonons but what is the functional form of this relationship?

In the case of a metal, the rate of energy transport, from electrons to phonons, is described by the power law³³

$$P_{e-ph} = V\Sigma(T_{el}^5 - T_{ph}^5), \quad (14)$$

where T_{el} is the electron temperature, T_{ph} the phonon temperature, and V the interaction volume. Σ is a material constant, and in the calculations reported in this paper, we used a value of $\Sigma=0.2 \times 10^9 \text{ W m}^{-3} \text{ K}^{-5}$ for Al, as measured using a Coulomb-blockade electrometer.³⁴ The volume was calculated through $V=wtl$, where w and l are the width and length of the microstrip line, and t is the thickness of the film. For an Al microstrip with the dimensions given in Table I, $V\Sigma=480 \text{ nW K}^{-5}$. The dashed line in Fig. 2 shows the power transported by electron-phonon coupling as a function of temperature, for a phonon temperature of 120 mK.

The system comes into equilibrium where the heating and cooling curves cross, and it is seen that multiple solutions can exist. As will be described, these different solutions give rise to hysteretic switching. A key point, however, is that although we might question whether Eq. (14) has the correct functional form for a superconductor, and whether the interaction volume should be reduced to account for the current density varying along the length of the resonator, the qualitative behavior remains unchanged. Widely varying

cooling curves result in the same generic behavior. We have carried out simulations using exponential cooling functions, and the same behavior is seen.

A further complication is that the Kapitza boundary conductance between the phonon system of the film and the phonon system of the substrate might affect the functional form of the cooling. Kapitza coupling is described by the power law

$$P_{Kap} = A\Sigma_{Kap}(T^4 - T_{bath}^4), \quad (15)$$

where $A=wl$ is the area of the microstrip line and Σ_{Kap} depends on the materials used. In general, this conductance needs to be added in series with that of the quasiparticle-phonon coupling. From Ref. 35 we estimate Σ_{Kap} to be $850 \text{ W m}^{-2} \text{ K}^{-4}$ and $A\Sigma_{Kap}=10 \mu\text{W K}^{-4}$, and therefore in the simulations that follow, we assume that the Kapitza conductance can be neglected.

A further possibility is that resonators are fabricated on thin ($<1 \mu\text{m}$) silicon nitride membranes for the purpose of increasing the quasiparticle lifetime, which has certain potential advantages for KIDs. The thermal transport properties of suspended membranes have been studied extensively in the context of low-noise Transition Edge Sensors. The thermal conductance of a mesoscopic dielectric support depends on a number of factors, including the dimensionality of the phonon system, which effectively varies with temperature. The power flow from a suspended membrane to the bath is described by

$$P_{mem} = K(T^n - T_{bath}^n), \quad (16)$$

where K is a geometry-dependent factor and n the power-law coefficient, which has been shown by a number of groups to have a value in the range 3–4, depending on the geometry and material used.^{36,37} Over the temperature range 50–300 mK, structures can be produced that have thermal conductances in the range 0.1 pWK^{-1} to 500 pWK^{-1} .

The key point about this discussion is that, for all of the mechanisms listed, the relationship between power flow and temperature takes the form of a simple power law. Thus, although the quantitative details will differ, Fig. 2 indicates that the different cooling functions will give rise to the same general behavior.

D. Steady state temperature

To this point we have said nothing about how the equilibrium temperature can be determined numerically. Calculating the steady-state temperature for different readout frequencies and power levels is equivalent to finding the intersection points of the heating and cooling curves in Fig. 2. For low readout power levels, the curves have only one intersection point, which occurs at temperatures very close to the bath temperature, and ideally, one would always operate a KID in this way.

For the readout power used in Fig. 2 (2 nW), however, the number of intersection points depends on the readout frequency. For the lowest frequencies, f_1 and lower, there is only one intersection point, which is close to the bath temperature. For high frequencies, f_4 and higher, there is again

only one intersection point but now it is significantly above the bath temperature. Frequencies in between show three intersection points, implying that there are three different solutions to the heat balance equation.

It is easy to show that the highest and lowest temperature solutions are stable but the middle one is not. Imagine that some external source of energy, or fluctuation such as generation-recombination noise, causes the temperature of the quasiparticle system to increase or decrease impulsively. Inspection of Fig. 2 shows that for the highest and lowest solutions, the temperature will relax back to its equilibrium state after the impulse has finished. The middle point, however, will either flip to the upper solution, because heating dominates cooling, or to the lower solution because cooling dominates heating, respectively.

In our simulation software, the steady-state temperatures were calculated, for every frequency, using a root-finding algorithm. The algorithm searches for the temperature that reduces the error $\xi(T) = P_{diss} - P_{e-ph}$ to zero. The iterative procedure

$$T_{k+1} = T_k - \gamma \frac{\partial T}{\partial \xi} \xi(T_k), \quad (17)$$

where T_k is the temperature at iteration k , is particularly effective because it has a quadratic rate of convergence near the solution. γ is a multiplicative constant having a value of between 0 and 1; typically 0.7. It determines the size of the step taken at each iteration, and its value does not affect the final solution but only the rate and stability with which the solution is found. Almost any guess can be used to initiate the procedure but in the case where some parameter is varied, say the readout frequency or readout power, the solution of the previous calculation can be used as the starting point of the next calculation.

For low power levels the implementation of the algorithm is straightforward since there is only one solution to the steady-state temperature, which is close to the bath temperature. In the case of multiple solutions, then by using the solution of the previous calculation, say when sweeping the frequency, as the starting guess of the next calculation, the procedure will follow the desired root in a smooth manner. Only when a root ceases to exist will the procedure switch to an available solution. Sweeping up or down in frequency leads to jumps, which as will be seen are hysteretic.

A calculation was performed using the algorithm described above for the Al resonator of Sec. II B, with a phonon temperature of 120 mK. The resulting quasiparticle temperature and transmission amplitude are plotted as a function of frequency in Figs. 3 and 4. The markers used are the same as those of Fig. 2, in the sense that a given symbol marks the point on Fig. 3, and Fig. 4, where the corresponding frequency curve of Fig. 2 has a solution by crossing the cooling curve. The solid symbols correspond to tracing the solution when the frequency is increasing (the low-temperature solutions), and the open symbols to the case when the frequency is decreasing (the high-temperature solutions).

The origin of the hysteresis in the resonance curve can be explained by comparing Fig. 2 with Figs. 3 and 4. Sweeping up in frequency means starting at a frequency f_1 or

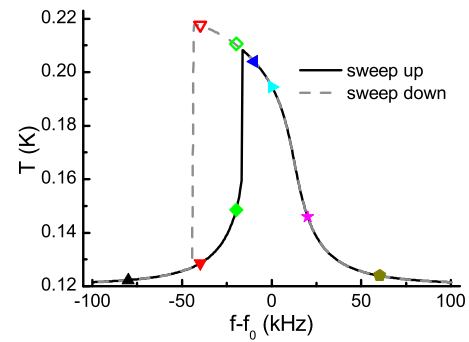


FIG. 3. (Color online) Steady-state temperature of the quasiparticles due to readout-power heating, assuming quasiparticle-phonon limited cooling. The markers correspond to the points of intersection of the heating and cooling curves in Fig. 2. The filled/open symbols show when the temperature is in the first/second stable state. The low temperature resonance frequency $f_0 = 4.263\ 02$ GHz.

lower, which has only one solution, close to the bath temperature. When the frequency is increased to f_2 , three solutions are possible, of which only the lowest and highest are stable, as discussed previously. If there are no large noise fluctuations, it can be assumed that at f_2 the system will remain in the low temperature state (indicated with a “ \blacktriangledown ”). The same situation prevails at f_3 , as indicated by the symbol “ \blacklozenge .” By f_4 the low-temperature state is unavailable, and the system switches to the high-temperature state, as indicated with the symbol “ \blacktriangleleft .” As a consequence, the resonance curve, Fig. 4, has a sharp downward transition. For frequencies f_5 to f_7 , the steady-state temperature decreases again, which completes the resonance curve for sweeping up in frequency. It is also clear that the noise spectrum of the readout signal will be altered significantly in the region close to the transition, an effect that is seen experimentally.

Sweeping down in frequency means starting at a frequency f_7 or higher, giving a steady-state temperature close to the phonon temperature. Frequencies f_6 , f_5 , and f_4 show an increasing temperature, until the region is reached where three solutions are available, f_3 . Again, assuming that the temperature noise levels are small, the quasiparticle system will initially be in the high-temperature state, marked with the symbol “ \blacklozenge ” in Fig. 2. By the time f_2 is reached, as marked by the symbol “ \blacktriangledown ,” a noise fluctuation is able to drive the instantaneous temperature below the middle state, and the system switches to the low-temperature state, as

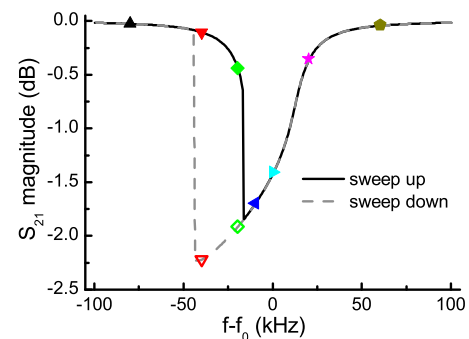


FIG. 4. (Color online) The resonator response curves, $|S_{21}|$, corresponding to the temperature curves in Fig. 3.

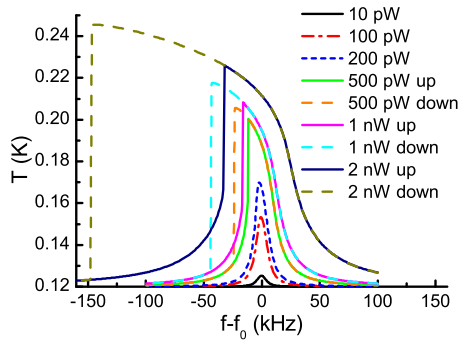


FIG. 5. (Color online) Calculated steady-state temperature of the quasiparticle system due to microwave heating for an Al microstrip resonator, shown as a function of frequency for different readout power levels and with $f_0 = 4.263\ 02\ \text{GHz}$.

shown in Fig. 3. The noise is no longer sufficient to switch it back. Interestingly, the overall Q of the resonator influences the exact frequency at which switching occurs. Finally, as the frequency comes down to f_1 and lower, only the low-temperature state is available, and the cycle is completed.

So far, σ_1 and σ_2 are calculated in every iteration step by numerically integrating Eqs. (1) and (2), and Δ is calculated by numerical inversion of Eq. (5). At low temperatures and frequencies, $\hbar\omega, kT \ll 2\Delta$, the integrals for σ_1 and σ_2 can be expressed analytically.³⁸ If one would also take a fixed value for Δ , P_{diss} can be expressed analytically. The steady state temperature still needs to be solved with a nonlinear solver but the procedure will be much faster. This analytical approach gives results reasonably close to the numerical strategy for $T/T_c < 0.2$. Since we did not want to limit ourselves to a certain temperature range, we used the full numerical approach for the calculations presented in this paper. We also performed a full set of simulations using the analytical formulae, which shows they are accurate to within 10% for the operation temperature and overestimate the power handling by only 3 dB, provided the temperature does not exceed $T/T_c = 0.2$.

III. EXTENDED SIMULATIONS

In this section we present an extended set of simulations, which explore additional features of the model.

A. Switching and hysteresis in the resonance curve

We have still to consider how the shape of the resonance curve changes as the readout power level is increased. In Figs. 5 and 6 the steady-state quasiparticle temperature and transmission amplitude of the Al resonator described previously are shown as a function of frequency for a set of readout powers. It can be seen that below 10 pW the internal temperature rise is small, and the resonance curve shows a deep symmetrical response. At 100 pW the quasiparticle temperature at resonance is already 30 mK above the phonon temperature, making the resonance curve less pronounced. At 200 pW there is a 50 mK temperature rise, and the resonance curve becomes asymmetrical. By 500 pW switching with hysteresis appears, with the hysteresis becoming more pronounced as the power is increased further.

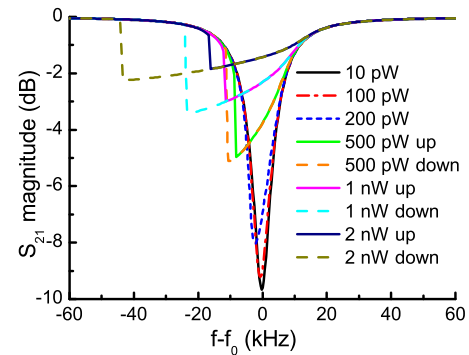


FIG. 6. (Color online) The resonator response curves, $|S_{21}|$, corresponding to the temperature curves in Fig. 5.

Since the phonon temperature appears in the power law for heat transport, Eq. (14), the power at which sufficient heating occurs for switching, decreases slightly if the phonon temperature is increased for the same resonator. If the phonon temperature is increased from 80 to 150 mK, switching occurs for the Al resonator at half the power level. The power threshold for switching will increase if the electron-phonon coupling (Σ) is stronger.

The power at which switching occurs increases with approximately the thickness squared in the simulations. The thickness dependence of the surface impedance and the thickness dependence in the heat transport law, Eq. (14), contribute to this dependence. In Fig. 6 for a 100 nm film, switching occurs at $-63\ \text{dBm}$ (500 pW) where for a 40 nm film, the switching occurs at $-71\ \text{dBm}$ and for 250 nm at $-59\ \text{dBm}$. The power handling decreases if the length of the resonator decreases (and the resonance frequency increases) because the dissipation volume decreases. In the frequency region of interest (1–10 GHz) there is no significant resonance frequency dependence if one leaves out the change in dissipation volume.

A higher conductivity of the film, σ_N (or a lower resistivity ρ), will lead to a decrease in resistive losses and therefore the power handling will be larger.

In general, the dissipated power into the quasiparticle system can be related to the readout power and quality factors by⁴ $P_{diss} = P_{readout}(2Q^2/Q_i Q_c)\chi_{qp}$, valid at resonance, where $\chi_{qp} = Q_i/Q_{i,qp}$ is the fraction of the dissipated power that goes into the quasiparticle system. In this paper we assumed $\chi_{qp} = 1$ as discussed in Sec. II B. This formula implies that the maximum readout power absorption occurs when $Q_i = Q_c$. If the quality factor is limited by coupling ($Q \approx Q_c \ll Q_i$), a lower Q_i will give a higher dissipation, leading to switching at lower readout powers.

B. Niobium and tantalum

The simulations reported so far have been limited to Al. Other materials, such as Nb ($T_c \approx 9\ \text{K}$) and Ta ($T_c \approx 4\ \text{K}$), are also interesting for KIDs, and so it is beneficial to explore their behavior. In fact we have performed a full set of simulations for these materials, and found the same general behavior as for Al.

Looking at the power law for quasiparticle-phonon limited heat transport, Eq. (14), we expect that for higher T_c

materials, more power is needed to set-up a significant temperature difference. Superconducting resonators are operated ideally at $T \approx T_c/10$.¹ For a Nb resonator with the same geometry as in Table I but with $N_0 V_{sc} = 0.306$, $T_D = 228$ K, $\rho = 14 \mu\Omega$ cm, and a phonon temperature of 1 K, the power needed to get sufficient heating for switching is 10 μ W (-20 dBm), assuming the same quasiparticle-phonon coupling. For a Ta resonator with the same geometry, and $N_0 V_{sc} = 0.25$, $T_D = 247$ K, $\rho = 13 \mu\Omega$ cm, and a phonon temperature of 0.4 K, the power needed for switching is 300 nW (-35 dBm), assuming the same quasiparticle-phonon coupling. Inspection of Eq. (14) shows that for a material with a higher T_c , the power that can be transported by electron-phonon coupling can be much higher, before a temperature of $T_c/5$ is reached. Therefore, the model predicts a higher power handling for materials with a higher T_c . The mentioned power levels for Nb and Ta are sufficiently high that another mechanism may cause the resonator to saturate, before the heating described here comes into effect. A detailed experimental study is needed before this question can be answered but it is interesting to note that Nb resonators show, experimentally, the same general behavior as our simulations predict.⁴²

C. Resonators on membranes

In Sec. II C, we mentioned the possibility of fabricating superconducting resonators on suspended silicon nitride membranes. The heat transported through thin legs can be described by $P_{mem} = K(T^m - T_{bath}^n)$, with $K = 10$ pW/K^{*n*} as an achievable but low value and *n* is about 3. The quasiparticle-phonon coupling and Kapitza coupling will generally be much greater, and therefore the most significant temperature difference will be between the membrane and bath. Using this new power law, with a bath temperature of 120 mK, the steady-state temperature of a membrane-supported Al KID was calculated for a number of readout power levels. The curves are the same as those in Fig. 6, only the power levels are different. Hysteretic switching is present for power levels of 200 fW and higher, which is three orders of magnitude lower than for the quasiparticle-phonon limited heat transport but high enough to operate as a detector.

IV. EXPERIMENTAL RESULTS

To illustrate the key features of readout-power heating, we present a set of experimental results that are characteristic of the behavior seen in many low- T_c materials, measured by a number of different groups. A 100 nm thick Al film was sputtered onto an R-plane sapphire substrate under ultra high vacuum conditions. The critical temperature of the film T_c was 1.228 K, the low temperature resistivity ρ was 0.63 $\mu\Omega$ cm, and the residual resistance ratio 5.2. A coplanar thin-film waveguide resonator was used in the experiment, and therefore we can only make a qualitative comparison with the simulations. The chip was cooled in a cryostat with an adiabatic demagnetization refrigerator to a bath temperature of 81 mK, and the complex transmission S_{21} was measured using a cooled high electron mobility transistor (HEMT) amplifier and a vector network analyzer.

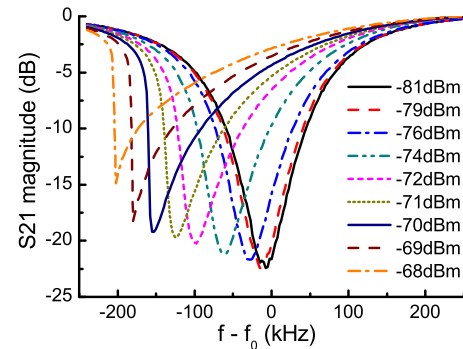


FIG. 7. (Color online) Experimental resonance curves of an Al coplanar waveguide resonator for different readout power levels. The bath temperature was 81 mK and $f_0 = 4.55929$ GHz.

$|S_{21}|$ is shown as a function of frequency in Fig. 7, for a range of readout power levels. Below -81 dBm, at the chip, the resonance curve was independent of the incident readout power, and it is in this range that a KID would normally be operated. A decrease in the absolute amplitude of the noise was observed as the readout power was increased, which is a well-known phenomenon. As the readout power was increased further, up to -70 dBm, the curve distorted, which is a sign of heating, because the resonance frequency shifts in the same direction as when the bath temperature is increased. Crucially at -69 dBm a discontinuity appeared. Although not shown here, because different apparatus had to be used to avoid blanking of the readout signal during frequency sweeping, it has also been confirmed that the resonance curves are hysteretic with the frequency interval between the switching events in the two sweep directions increasing as the power level is increased. It was also observed that the spectrum of the noise fluctuations on $|S_{21}|$ changed markedly when the device was read out at a single frequency close to one of the discontinuities. All of these observations are consistent with the phenomena predicted by our simple model.

V. DISCUSSION

The major assumption behind the simple model developed in this paper is that the quasiparticle distribution under microwave absorption can be described as a thermal distribution at elevated temperature. Second, that the limited electron-phonon transport, which leads to the elevated temperature, can be described by a power law. Although the nonlinear behavior is well described by this model, the description of the microwave absorption can be refined, to correctly account for the microscopic properties of the superconductor. The microwave field in the resonator varies along the length of the resonator and therefore microwave absorption will have a spatial dependence. Eliashberg and co-workers^{39,40} formulated the rate at which the quasiparticle distribution is changed by the vector potential of the microwave field. Given this rate of change, the framework of Chang and Scalapino⁴¹ provides a way to calculate the steady state quasiparticle- and phonon distributions in the superconductor if the electron-phonon coupling and the phonon escape time in the film are known. In future research, we will include this framework, together with the spatially vary-

ing field, into the model and compare it with the thermal approximation we made here. The framework may also be used to model and optimize the detector sensitivity.⁴

Because the work reported here was undertaken to establish the principles of the approach, the simulations were carried out using the loss equations of a microstrip line, which are particularly straightforward to use. Similarly accurate equations for coplanar line are not readily available. Also, we have used a cooling curve that was formulated for normal metals rather than superconductors, and therefore it is not possible to perform a detailed numerical comparison. It is essential to appreciate, however, that the key elements of the model follow directly from the general shape of the power-absorption curve of the resonator, and the general shape of the cooling curve of the quasiparticle system; the observed behavior does not depend in a critical way on experimental parameters. The current distributions, and therefore the losses in the two geometries, are not dramatically different, and therefore we would expect the power levels at which the effects are seen to be of the same order of magnitude.

We also assumed a volume $V=wtl$ in which the microwave power is dissipated and the electron-phonon transport takes place. The microwave field only extends about the distance of the penetration depth into the metal, which is around 80 nm for Al, of the order of the film thickness. However, the quasiparticle diffusion time on the scale of the strip width (3 μm) is less than a nanosecond. Since the relaxation processes are slower, the assumption of uniform electron-phonon transport over the strip cross-section is justified. On the length of the strip, the current distribution is proportional to $\cos^2(x)$, with x the coordinate along the length of the strip. Since this is a smoothly rising function, we estimate the error of taking the whole length of the strip to be a factor of 2 at maximum.

We have assumed that dielectric loss is not present at any significant level but we did restrict the Q_i to some maximum value Q_{sat} , and it is known that dielectric loss decreases with increased power.³⁰ If dielectric loss, or even radiation loss, is present then we might expect switching to occur at a slightly higher readout power. Power dissipation in the superconductor and the dielectric could be distinguished in the model. From the simulations we would expect that switching, in the case of quasiparticle-phonon limited transport, for a 100 nm thick film, to be present for powers higher than -63 dBm (500 pW), whereas we get a value of -69 dBm (125 pW) from the measurements presented in Fig. 7. Given the assumptions made, these are pleasingly similar. We are currently carrying out a detailed quantitative study, comparing simulated resonance curves with experimental measurements on films having different thicknesses (10–100 nm), and these will be reported shortly.

The resonance curves presented in Fig. 7 are representative of all of the superconducting resonators we have measured over a number of years: many Nb, Ta, and Al resonators on a variety of substrates, in a number of different cryogenic systems. Although the results are quantitatively different they are all qualitatively the same. The only difference was in a single measurement on a Nb resonator, when two discontinuities were seen when sweeping the frequency

in the same direction.⁴² This observation can now be understood in terms of an inadvertent double-dip on the power absorption curve of the resonant circuit, leading to three stable and two unstable quasiparticle temperature states.

If it is demonstrated that the mechanism described in this paper is responsible for the observed behavior of KIDs, as distinct from say exceeding the critical current at the edges of the film, where the current density is high, then the heating model will be of considerable importance. For example, it is interesting to observe that if we can calculate the power absorption curve of the resonator accurately, then it should be possible to recover, from large-signal measurements of resonance curves, the precise functional form of the quasiparticle-phonon cooling function, which would be of great interest in its own right. Both the distortion of the resonance curve, and the frequencies of the switching events, can be used to uncover information about the microscopic physics involved.

An alternative approach is to measure the scattering parameters, both S_{11} and S_{21} , as a function of bath temperature for low readout powers, and thereby calculate the absorbed power as a function of bath temperature. Assuming that the observed heating is the same as when power is absorbed by the quasiparticle system directly, then the cooling curve can be recovered from high readout-power measurements at the bath base temperature, without the need for microwave simulations.

VI. CONCLUSIONS

We have presented a model for nonlinear behavior due to readout-power heating in KIDs. It has been shown that the power dissipated in a superconducting resonator, as a function of temperature, has a peak such that when combined with a typical monotonically increasing cooling curve, leads to two stable and one unstable quasiparticle temperature states. The exact form of the cooling curve, whether due to quasiparticle-phonon coupling or Kapitza boundary effects, does not change the general form of what is seen: at low power levels, the intrinsic behavior of the resonator is measured, at medium power levels, the resonance curve distorts, and at high power levels, switching appears. The switching is hysteretic in the frequency domain, and the frequency difference between the transition points increases as the readout power is increased. All of these effects are seen in both the simulations and in experiments.

Not only is our model potentially important for optimizing the behavior of KIDs, it may also open the door to interesting physics. For example, it should be possible to recover the precise functional form of the cooling mechanism. The work also shows that it should be possible to operate resonators on suspended membranes, and therefore it should be possible to study the way in which the cooling changes as a function of the dimensionality of the phonon system of the substrate.

Intriguingly, using the hysteresis, it may be possible to make a photon-counting detector that latches after an event has occurred, and which is then reset by offsetting the frequency of the readout source.

ACKNOWLEDGMENTS

This work was carried out during three months a visit of Pieter de Visser to the Department of Physics at the University of Cambridge, which was partially financed by an Erasmus grant. We thank T. M. Klapwijk for valuable discussion.

- ¹P. K. Day, H. G. LeDuc, B. A. Mazin, A. Vayonakis, and J. Zmuidzinas, *Nature (London)* **425**, 817 (2003).
- ²J. Gao, M. Daal, J. M. Martinis, A. Vayonakis, J. Zmuidzinas, B. Sadoulet, B. A. Mazin, P. K. Day, and H. G. Leduc, *Appl. Phys. Lett.* **92**, 212504 (2008).
- ³R. Barends, H. L. Hortensius, T. Zijlstra, J. J. A. Baselmans, S. J. C. Yates, J. R. Gao, and T. M. Klapwijk, *IEEE Trans. Appl. Supercond.* **19**, 936 (2009).
- ⁴H. G. Leduc, B. Bumble, P. K. Day, B. H. Eom, J. Gao, S. Golwala, B. A. Mazin, S. McHugh, A. Merrill, D. C. Moore, O. Noroozian, A. D. Turner, and J. Zmuidzinas, *Appl. Phys. Lett.* **97**, 102509 (2010).
- ⁵J. Gao, L. R. Vale, J. A. B. Mates, D. R. Schmidt, G. C. Hilton, K. D. Irwin, F. Mallet, M. A. Castellanos-Beltran, K. W. Lehnert, J. Zmuidzinas, and H. G. Leduc, arXiv:1008.0046v1 (unpublished).
- ⁶A. V. Velichko, M. J. Lancaster, and A. Porch, *Supercond. Sci. Technol.* **18**, R24 (2005).
- ⁷A. Gurevich and R. Mints, *Rev. Mod. Phys.* **59**, 941 (1987).
- ⁸J. Wosik, L.-M. Xie, K. Nesteruk, D. Li, J. H. Miller, and S. A. Long, *J. Supercond.* **10**, 97 (1997).
- ⁹P. Lahl and R. Wördenweber, *J. Appl. Phys.* **97**, 113911 (2005).
- ¹⁰M. A. Golosovsky, H. J. Snortland, and M. R. Beasley, *Phys. Rev. B* **51**, 6462 (1995).
- ¹¹B. Abdo, E. Sergev, O. Shtempluch, and E. Buks, *J. Appl. Phys.* **101**, 083909 (2007).
- ¹²D. E. Oates, P. Nguyen, G. Dresselhaus, M. S. Dresselhaus, C. W. Lam, and S. M. Ali, *J. Supercond.* **5**, 361 (1992).
- ¹³J. H. Oates, R. T. Shin, D. E. Oates, M. J. Tsuk, and P. P. Nguyen, *IEEE Trans. Appl. Supercond.* **3**, 17 (1993).
- ¹⁴T. Dahm and D. J. Scalapino, *J. Appl. Phys.* **81**, 2002 (1997).
- ¹⁵B. Yurke and E. Buks, *J. Lightwave Technol.* **24**, 5054 (2006).
- ¹⁶E. A. Tholén, A. Ergül, E. M. Doherty, F. M. Weber, F. Grégis, and D. B. Haviland, *Appl. Phys. Lett.* **90**, 253509 (2007).
- ¹⁷C. C. Chin, D. E. Oates, G. Dresselhaus, and M. S. Dresselhaus, *Phys. Rev. B* **45**, 4788 (1992).
- ¹⁸G. Ghigo, R. Gerbaldo, L. Gozzelino, F. Laviano, G. Lopardo, E. Monticone, C. Portesi, and E. Mezzetti, *Appl. Phys. Lett.* **94**, 052505 (2009).
- ¹⁹R. Monaco, A. Andreone, and F. Palomba, *J. Appl. Phys.* **88**, 2898 (2000).
- ²⁰J. Wosik, L. M. Xie, R. Grabovickic, T. Hogan, and S. A. Long, *IEEE Trans. Appl. Supercond.* **9**, 2456 (1999).
- ²¹J. Kermorvant, C. J. van der Beek, J.-C. Mage, B. Marcilhac, Y. Lemaître, J. Briatico, R. Bernard, and J. Villegas, *J. Appl. Phys.* **106**, 023912 (2009).
- ²²L. F. Cohen, A. L. Cowie, A. Purnell, N. A. Lindop, S. Thiess, and J. C. Gallop, *Supercond. Sci. Technol.* **15**, 559 (2002).
- ²³B. Abdo, E. Segev, O. Shtempluch, and E. Buks, *Appl. Phys. Lett.* **88**, 022508 (2006).
- ²⁴R. Vijay, M. H. Devoret, and I. Siddiqi, *Rev. Sci. Instrum.* **80**, 111101 (2009).
- ²⁵D. C. Mattis and J. Bardeen, *Phys. Rev.* **111**, 412 (1958).
- ²⁶R. L. Kautz, *J. Appl. Phys.* **49**, 308 (1978).
- ²⁷G. Yassin and S. Withington, *J. Phys. D: Appl. Phys.* **28**, 1983 (1995).
- ²⁸J. M. Martinis, M. Ansmann, and J. Aumentado, *Phys. Rev. Lett.* **103**, 097002 (2009).
- ²⁹R. Barends, J. J. A. Baselmans, J. N. Hovenier, J. R. Gao, S. J. C. Yates, T. M. Klapwijk, and H. F. C. Hoevers, *IEEE Trans. Appl. Supercond.* **17**, 263 (2007).
- ³⁰J. Gao, M. Daal, A. Vayonakis, S. Kumar, J. Zmuidzinas, B. Sadoulet, B. A. Mazin, P. K. Day, and H. G. Leduc, *Appl. Phys. Lett.* **92**, 152505 (2008).
- ³¹R. Barends, N. Vercruyssen, A. Endo, P. J. de Visser, T. Zijlstra, T. M. Klapwijk, P. Diener, S. J. C. Yates, and J. J. A. Baselmans, *Appl. Phys. Lett.* **97**, 023508 (2010).
- ³²R. D. Parks, *Superconductivity*, 1st ed. (M. Dekker, New York, 1969), Vol. 2.
- ³³F. C. Wellstood, C. Urbina, and J. Clarke, *Phys. Rev. B* **49**, 5942 (1994).
- ³⁴R. L. Kautz, G. Zimmerli, and J. M. Martinis, *J. Appl. Phys.* **73**, 2386 (1993).
- ³⁵E. T. Swartz and P. O. Pohl, *Rev. Mod. Phys.* **61**, 605 (1989).
- ³⁶T. Kühn, D. V. Anghel, J. P. Pekola, M. Manninen, and Y. M. Galperin, *Phys. Rev. B* **70**, 125425 (2004).
- ³⁷K. Rostem, D. J. Goldie, S. Withington, D. M. Glowacka, V. N. Tsaneva, and M. D. Audley, *J. Appl. Phys.* **105**, 084509 (2009).
- ³⁸J. Gao, J. Zmuidzinas, A. Vayonakis, P. Day, B. Mazin, and H. Leduc, *J. Low Temp. Phys.* **151**, 557 (2008).
- ³⁹G. M. Eliashberg, *JETP Lett.* **11**, 114 (1970).
- ⁴⁰B. I. Ivlev, S. G. Lisitsyn, and G. M. Eliashberg, *J. Low Temp. Phys.* **10**, 449 (1973).
- ⁴¹J.-J. Chang and D. J. Scalapino, *Phys. Rev. B* **15**, 2651 (1977).
- ⁴²G. Vardoulakis, "Superconducting kinetic inductance detectors, theory, simulations, and experiments," Ph.D. thesis, University of Cambridge, 2007.